nature neuroscience

SUPPLEMENTARY INFORMATION

https://doi.org/10.1038/s41593-018-0109-1

In the format provided by the authors and unedited.

A three-dimensional single-cell-resolution whole-brain atlas using CUBIC-X expansion microscopy and tissue clearing

Tatsuya C. Murakami[1], Tomoyuki Mano[1,2], Shu Saikawa[3], Shuhei A. Horiguchi[4,5], Daichi Shigeta[1], Kousuke Baba[6,7], Hiroshi Sekiya[8], Yoshihiro Shimizu[9], Kenji F. Tanaka[10], Hiroshi Kiyonari[11], Masamitsu Iino[8,12], Hideki Mochizuki[6], Kazuki Tainaka[1,13] and Hiroki R. Ueda[1,2,4]*

[1]Department of Systems Pharmacology, Graduate School of Medicine, The University of Tokyo, Tokyo, Japan. [2]International Research Center for Neurointelligence (WPI-IRCN), UTIAS, The University of Tokyo, Tokyo, Japan. [3]Department of Computational Biology and Medical Sciences, Graduate School of Frontier Sciences, The University of Tokyo, Chiba, Japan. [4]Laboratory for Synthetic Biology, RIKEN Quantitative Biology Center, Osaka, Japan. [5]Department of Systems Science, School of Engineering Science, Osaka University, Osaka, Japan. [6]Department of Neurology, Graduate School of Medicine, Osaka University, Osaka, Japan. [7]Department of Kampo Medicine, Graduate School of Medicine, Osaka University, Osaka, Japan. [8]Department of Pharmacology, Graduate School of Medicine, The University of Tokyo, Tokyo, Japan. [9]Laboratory for Cell-Free Protein Synthesis, RIKEN Quantitative Biology Center, Osaka, Japan. [10]Department of Neuropsychiatry, Keio University School of Medicine, Tokyo, Japan. [11]Animal Resource Development Unit and Genetic Engineering Team, RIKEN Center for Life Science Technologies, Kobe, Japan. [12]Division of Cellular and Molecular Pharmacology, Nihon University School of Medicine, Tokyo, Japan. [13]Brain Research Institute, Niigata University, Niigata, Japan. *e-mail: uedah-tky@umin.ac.jp

a

		PBS	Water	Ionic: Guanidine hydrochloride (GH)	Ionic: Sodium deoxycholate (SD)	Tween20	Nonident P-40	Triton X-100	Acetonitrile	DMF	DMA	1,4-Dioxane	DMSO	Urea derivative: Urea	Urea derivative: Thiourea
Brain	Average	0.847	1.514	0.553	0.774	1.219	1.361	1.412	1.541	1.542	1.585	1.614	1.673	1.714	1.896
	SD	0.021	0.004	0.001	0.003	0.005	0.063	0.005	0.075	0.024	0.012	0.017	0.056	0.037	0.031
Gelatin	Average	0.999	1.544	0.798	0.808	1.113	1.215	1.251	1.473	1.541	1.496	1.516	1.473	1.616	1.458
	SD	0.022	0.041	0	0.008	0.024	0.02	0.033	0.046	0.075	0.07	0.061	0.134	0.064	0.047

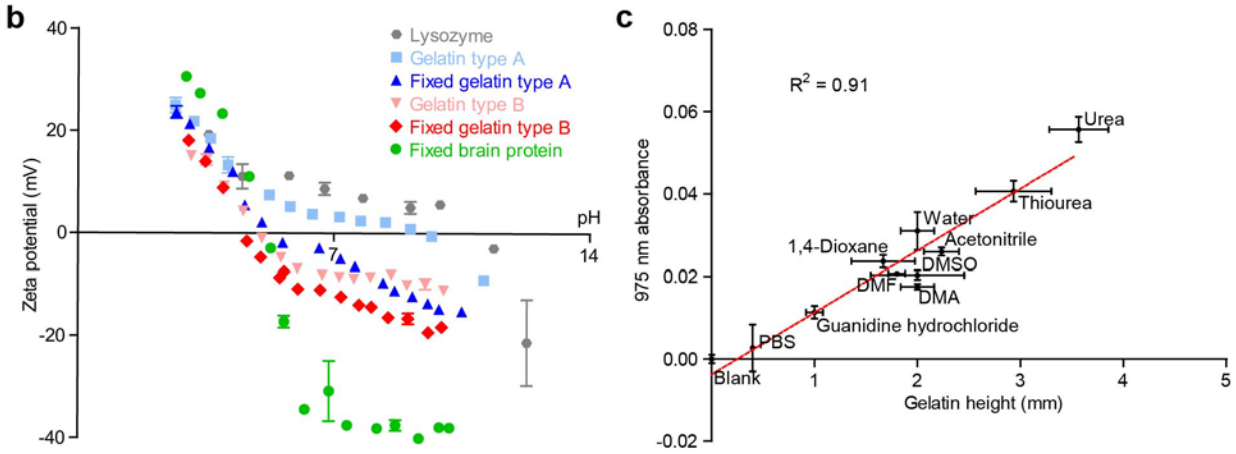

Supplementary Figure 1

Development of gelatin-based high-throughput screening assay.

(a) The swelling ratio (the average and SD) of chemically treated brain samples and gelatin gel between before and after chemical treatment shown in Fig. 1a (brain; n = 2, gelatin; n = 3). All chemicals are chosen from our previous study (Online Methods). Urea derivatives (blue color) remarkably swelled brain samples compared to ionic chemicals (red color). (b) The plots of zeta potential against pH for various protein samples. Each zeta potential curve was fitted to fourth-order polynomials. The isoelectric points were determined by calculating crossing points of polynomials with the x-axis. The measurements were repeated three times at each pH point. (c) Correlation of the 975 nm absorbance and apparent height of type B gelatin (n = 3) treated with PBS, water, or 8 other chemicals indicated in the panel. The 975 nm absorbance of chemically treated gelatin gels showed a linear correlation with the apparent height of those. R-squared value was calculated with all data plots. All values are mean ± SD.

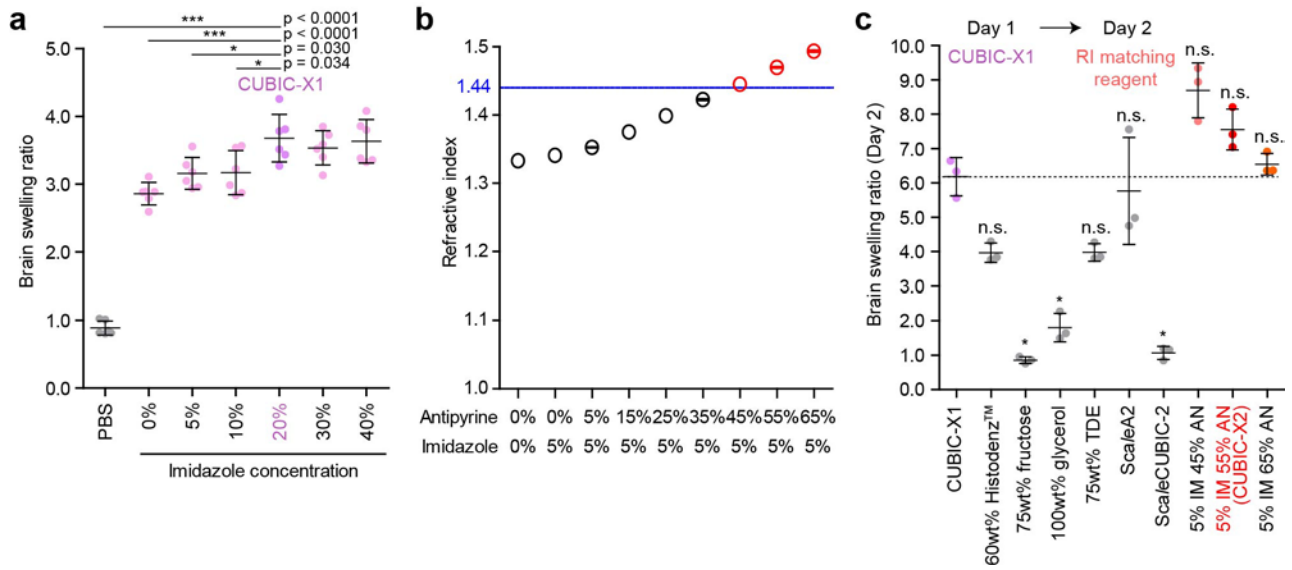

Supplementary Figure 2

CUBIC-X1 and CUBIC-X2 for whole-brain expansion and hyperhydrative RI matching.

(a) Swelling ratios of delipidated hemisphere brains treated by imidazole aqueous solutions for 1 day. Delipidated hemisphere brains were immersed in various concentration of imidazole aqueous solutions (n = 6). The 20% imidazole solution, termed CUBIC-X1, was the minimal concentration to achieve the largest expansion volume (***p < 0.001, *p < 0.05, one-way ANOVA, Tukey's post hoc test for multiple comparisons). (b) Refractive indices of cocktails of imidazole and antipyrine (n = 3). We note that the standard error of several points cannot be shown because those measured values rounded at third decimal place resulted in the identical values. (c) Swelling ratios of hemisphere brains by RI matching media. Delipidated hemisphere brains were treated with CUBIC-X1 for 1 day, and then immersed in various kinds of RI media for 1 day (n = 3, *p < 0.05, Dunnett's Modified Tukey-Kramer pairwise multiple comparison test). All values are mean ± SD.

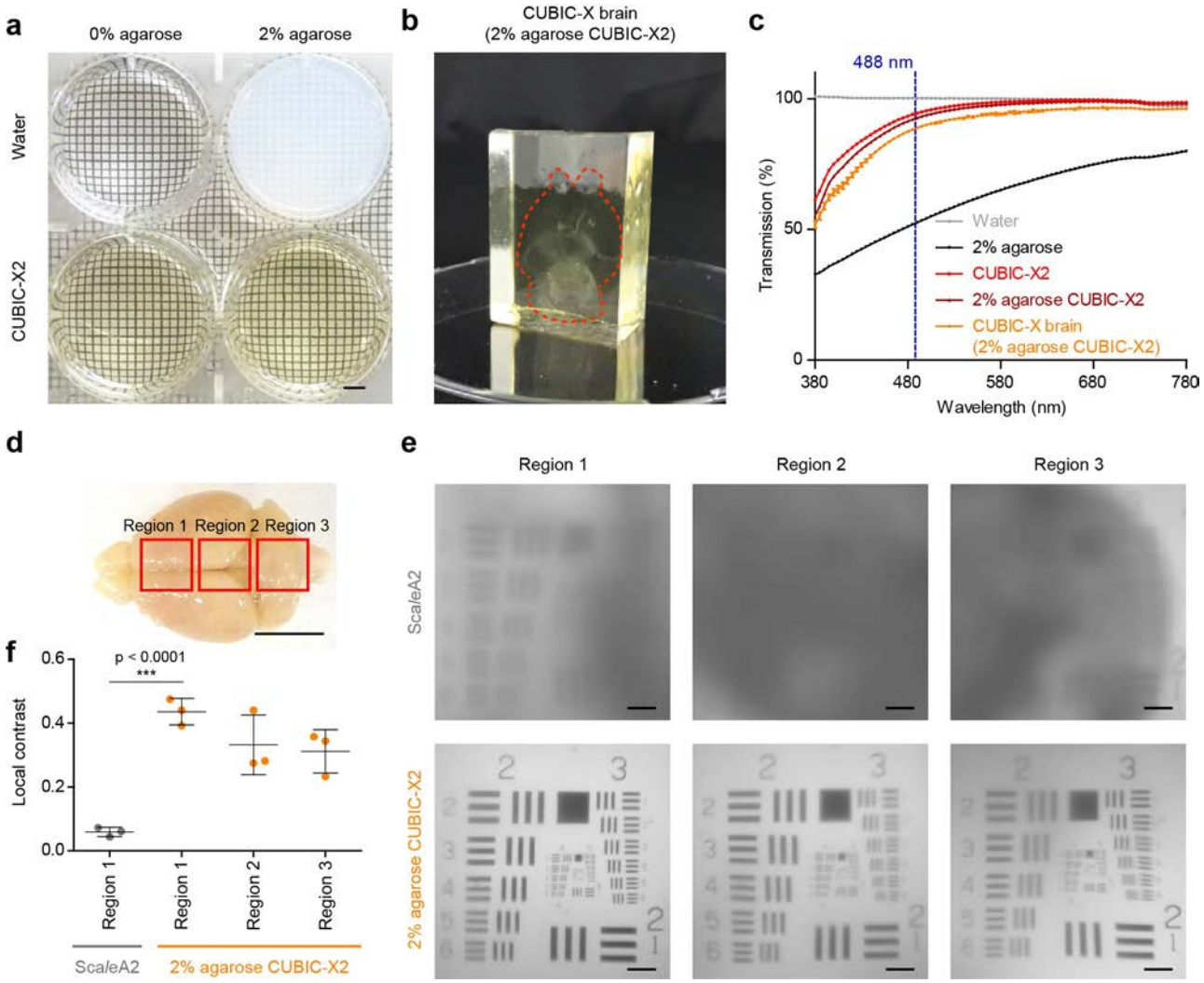

Supplementary Figure 3

Embedding of a CUBIC-X brain into an agarose gel.

(a) Transmission images of water, CUBIC-X2, 2% agarose, and 2% agarose CUBIC-X2. 2% agarose CUBIC-X2 showed high transparency while 2% agarose showed white turbidity. (b) Image of a CUBIC-X brain (2% agarose CUBIC-X2). The gel embedded expanded brain was highly transparent and solid enough to mount on the LSFM. (c) Transmission curves of water, CUBIC-X2, 2% agarose, 2% agarose CUBIC-X2, and CUBIC-X brain (2% agarose CUBIC-X2). Light transmittance around the visible region (380-780 nm) was measured (n = 3). (d) Three regions of the brain quantified in e. (e) ScaleA2 and CUBIC-X2 treated CUBIC-X1 expanded brains were placed on USAF chart for quantitative analysis of scattering. The CUBIC-X2 brains were embedded in 2% agarose. (f) Comparison of the local contrasts of the ScaleA2 and CUBIC-X2 treated CUBIC-X1 expanded brains. The local contrasts were quantified by referring local intensity profiles over element 2, group 2 of USAF chart (Online Methods, n = 3, ***p < 0.001, independent two-tailed t-test). All values are mean ± SD. Scale bars indicate 5 mm (a, d) and 500 μm (e).

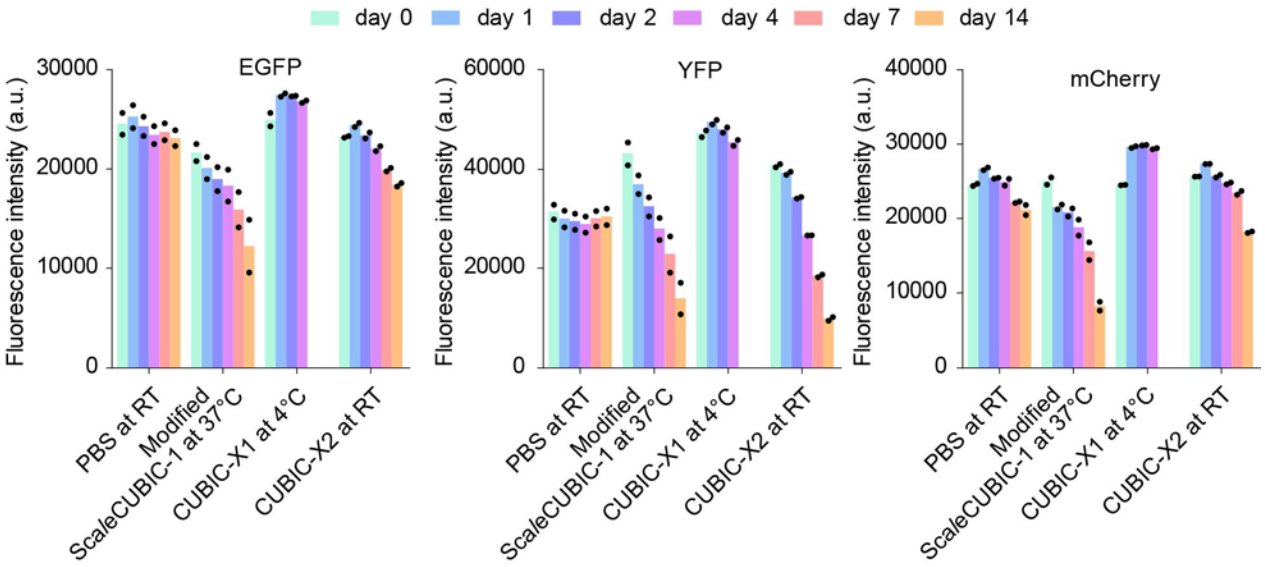

Supplementary Figure 4

Intensity of fluorescent proteins in various CUBIC solutions.

Quenching test of fluorescent proteins by several CUBIC reagents. The indicated recombinant fluorescent proteins were incubated in each reagent or PBS for up to two weeks. The bars indicate the averages (n = 2).

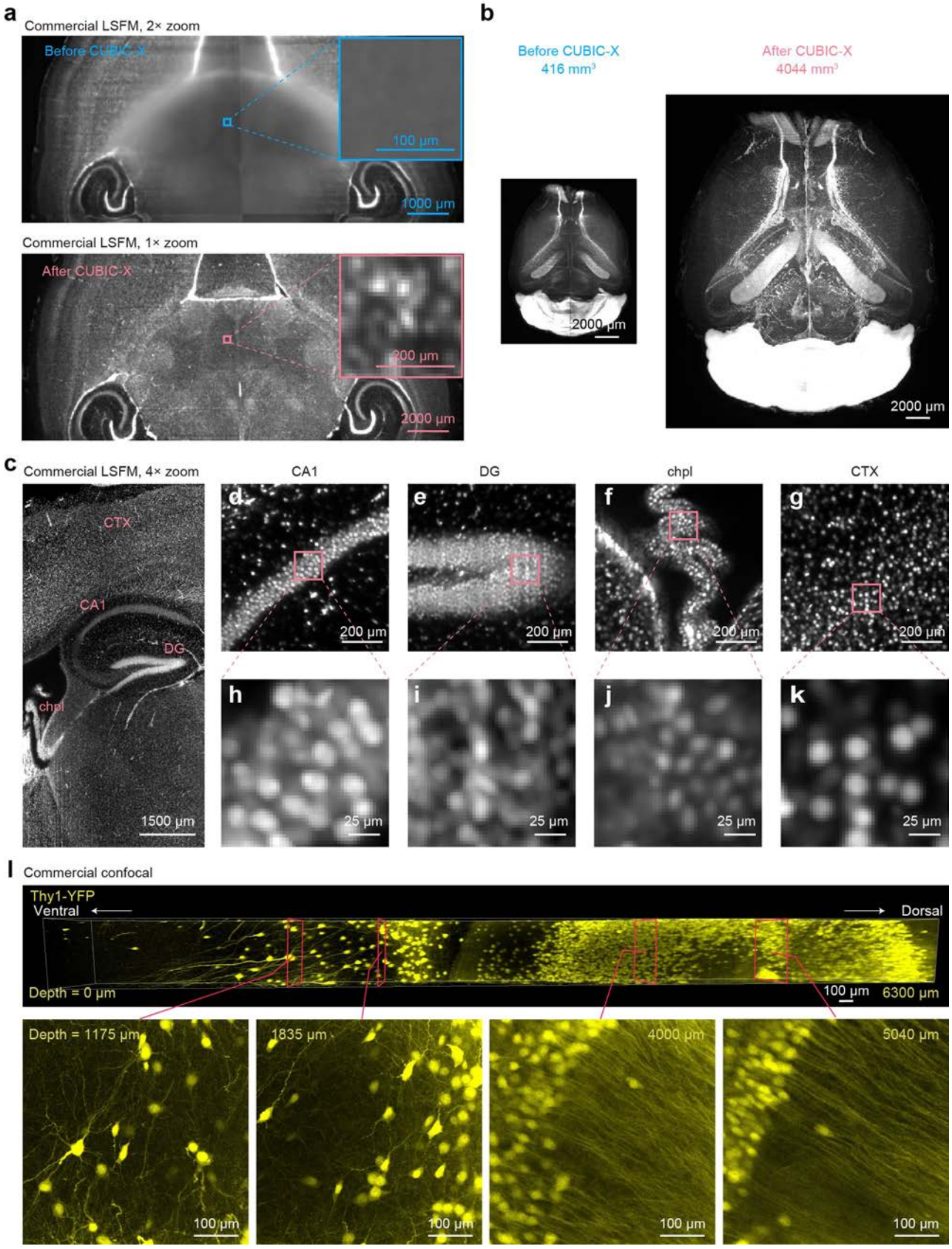
a
Commercial LSFM, 2× zoom
Before CUBIC-X
100 μm
1000 μm
Commercial LSFM, 1× zoom
After CUBIC-X
200 μm
2000 μm
b
Before CUBIC-X
416 mm³
After CUBIC-X
4044 mm³
2000 μm
2000 μm
c
Commercial LSFM, 4× zoom
CTX
CA1
DG
chpl
1500 μm
CA1
DG
chpl
CTX
d
e
f
g
200 μm
200 μm
200 μm
200 μm
h
i
j
k
25 μm
25 μm
25 μm
25 μm
l
Commercial confocal
Thy1-YFP
Ventral
Dorsal
Depth = 0 μm
100 μm
6300 μm
Depth = 1175 μm
1835 μm
4000 μm
5040 μm
100 μm
100 μm
100 μm
100 μm

Supplementary Figure 5

CUBIC-X brain images acquired by commercial LSFM and commercial confocal microscopy.

(a) Using a commercial LSFM, a low-magnification images of a PI-stained brain before (upper) and after (lower) CUBIC-X were obtained with 2× and 1× zoom lens, respectively (Online Methods). Insets: magnified views of the brains. (b) Volume-rendered images of a PI-stained brain before (left) and after (right) CUBIC-X in the same scale. Volumes were quantified by segmenting the brains (Online Methods). (c) PI-stained brain after CUBIC-X treatment was imaged with commercial LSFM with 4× magnification. To generate a virtual thin light sheet, four images with different light sheet focus positions were tiled together. DG: dentate gyrus, chpl: Choroid plexus, CTX: Cerebral cortex. (d-g) Magnified views of representative regions in brain. (h-k) Magnified views of d,e,f,g, respectively. (l) Fluorescent protein imaging of a Thy1-YFP-H mouse brain with a commercial confocal microscope. A Thy1-YFP-H mouse brain was cleared and expanded with CUBIC-X protocol, and imaged with confocal microscopy (25×, NA = 1.0). The volume rendered image (an upper panel; a volume size of 0.5 mm × 0.5 mm × 6.3 mm) and images of maximum-intensity projections (lower panels; 225 μm, 225 μm, 10 μm, 10 μm in thickness from left) are visualized. For all panels, experiments were repeated three times with independent brains. The representative images are shown.

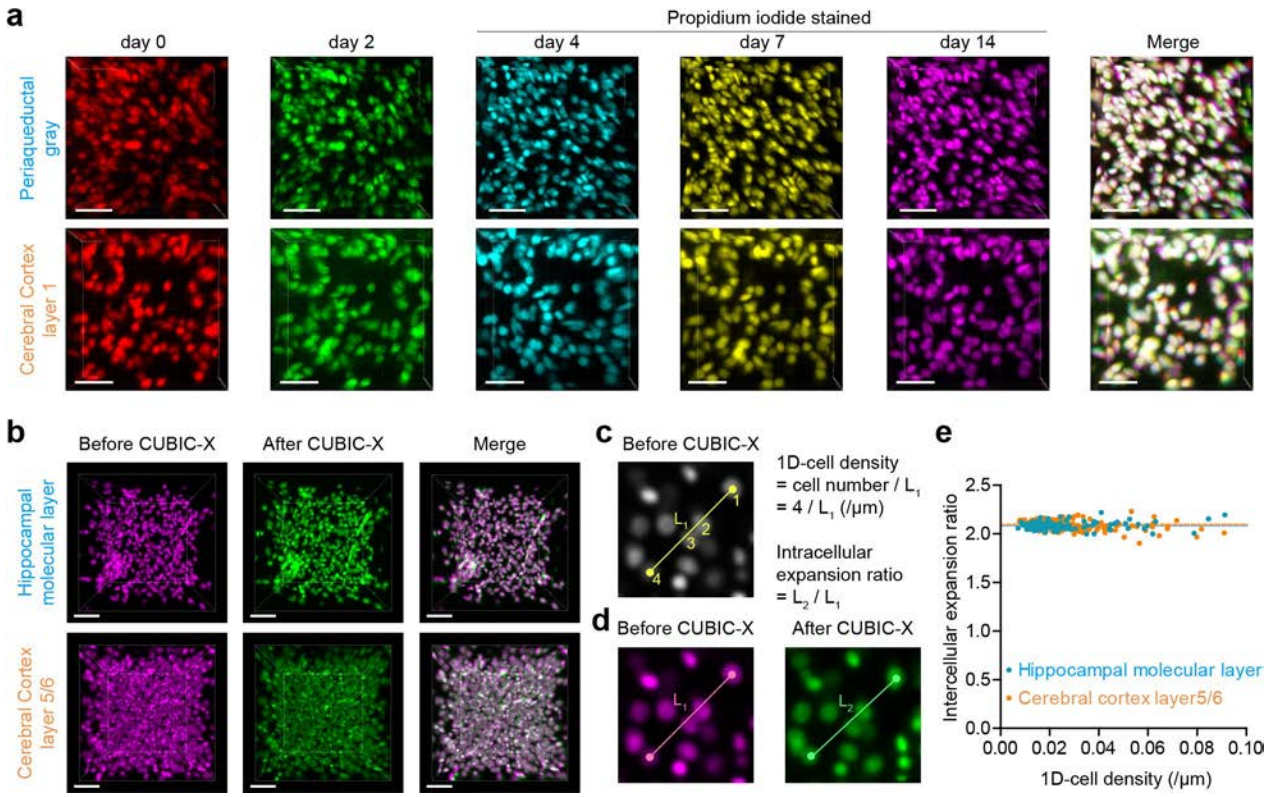

Supplementary Figure 6

Multi-cellular scale evaluation of distortion and cellular loss during delipidation and expansion procedures.

(a) Sequential observation of nuclei during the delipidation process. The sliced brains of R26-H2B-EGFP mice were observed prior to the delipidation process (day 0). The slices were repeatedly observed during the delipidation process (day 2, 4, 7 and 14). Because repeated observation with fluorescence microscopy bleaches EGFP signal, propidium iodide was added at day 3 to enhance the signal of nuclei. Two regions of the brains (periaqueductal gray and cerebral cortex layer 5/6) are shown. Scale bars indicate 25 μm in the scale of a “before-CUBIC-X” brain. (b) Multi-cellular scale comparison of “before-CUBIC-X” brain and “after-CUBIC-X” brain. Two regions (hippocampal molecular layer and cerebral cortex layer 5/6) are shown. The corresponding images of “after-CUBIC-X” brain, which were linearly registered to “before-CUBIC-X” brain images by affine transformation, are also shown (Online Methods). It was confirmed that none of the nuclei were lost in the investigated area. The merged images after registration are shown on the right. Scale bars indicate 50 μm in the scale of a “before-CUBIC-X” brain. In (a) and (b), a perspective 3D rendering was used by Imaris software for visualization. Experiments were repeated three times with independent brain slices or brains. The representative images are shown. (c,d) Schematic procedures of the measurement of 1D-cell density (c) and intercellular expansion ratio (d). 1D-cell density was measured for every pair of cells by counting the number of nuclei between the pair. Intercellular expansion ratio was calculated for every pair of cells as L2/L1. For the analysis, images of “after-CUBIC-X” were registered to images of “before-CUBIC-X” by similarity transformation. (e) The relation between 1D-cell density and Intercellular expansion ratio. Blue and orange dashed lines indicate overall expansion ratios in hippocampal molecular layer and cerebral cortex layer 5/6, respectively.

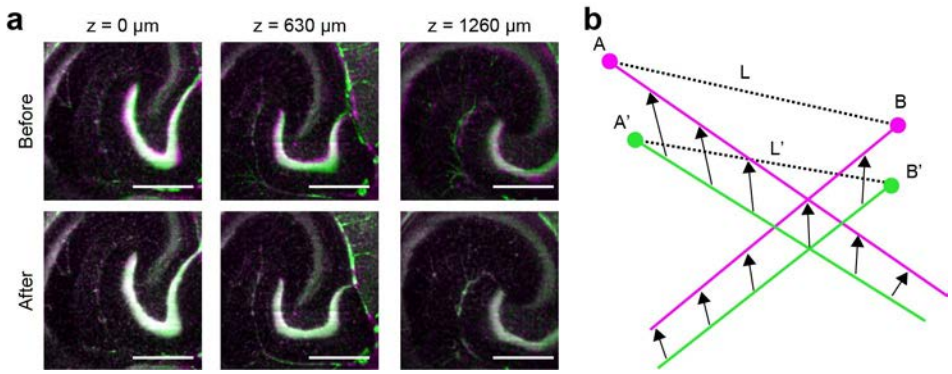

Supplementary Figure 7

Global scale evaluation of distortion during expansion procedures.

(a) Comparison of merged images of “before-CUBIC-X” (magenta) and “after-CUBIC-X” (green) brain between before- and after-non-linear transformation. After linear registration by affine transformation, three horizontal images were merged in the hippocampal region (2.5 mm × 2.5 mm × 2.5 mm) of a “before-CUBIC-X” (magenta) brain to the corresponding images of an “after-CUBIC-X” (green) brain in the upper row. After further non-linear transformation, the corresponding images are shown in the lower row. Scale bars indicate 500 μm in the scale of a “before-CUBIC-X” brain. (b) Schematic procedures of the measurement of root-mean-square (RMS) error value in Fig. 3b. L’ and L were calculated by measuring the Euclidean distance between two points of before non-linear registration (shown as A’ and B’) and after non-linear registration (shown as A and B), respectively. Both of L’ and L were measured in the scale of the before non-linear transformed image.

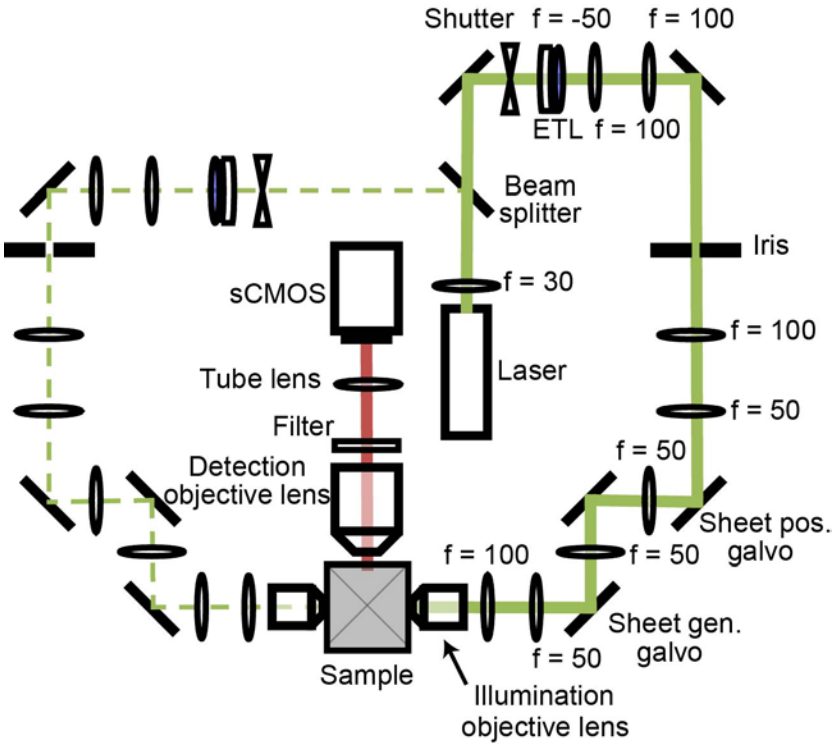

Supplementary Figure 8

Optical layout of the customized light sheet microscope.

Electrically tunable lenses (ETL) were put for the adjustment of the light-sheet focus position along the x-direction. Galvanometer scanners were introduced for adjusting a light-sheet position along z-direction (shown as “sheet pos. galvo”). Autofocus (i.e. adjustment of the light-sheet z-position) by these galvanometer scanners was performed every 1 mm.

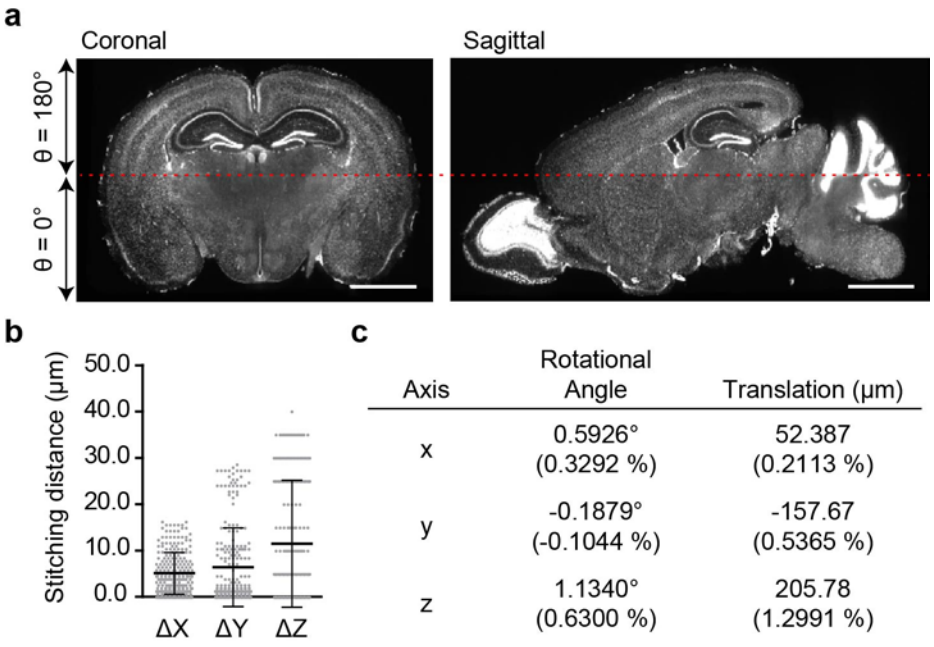

Axis	Rotational Angle	Translation (μm)
x	0.5926° (0.3292 %)	52.387 (0.2113 %)
y	-0.1879° (-0.1044 %)	-157.67 (0.5365 %)
z	1.1340° (0.6300 %)	205.78 (1.2991 %)

Supplementary Figure 9

Quantitative measurements of the displacements during the imaging sequence.

(a) Coronal and sagittal image merged by θ-rotation with dorsal (θ = 0°) and ventral (θ = 180°) sides of the CUBIC-X brain. Red dashed line is the merged position. Scale bars indicate 2000 μm in the scale of a “before-CUBIC-X” brain. (b) Quantitative evaluation of stitching displacement errors in x, y, and z-axes in the xy-direction tiling. We prepared 10 × 10 tiles of 600 images for each stack with 10% overlap in both x- and y-direction. Stitching distance was calculated with the stitching software, TeraStitcher. The displacement errors of all possible combinations of the stacks are shown. The average ± SD are shown. (c) Quantitative evaluation of theta tile displacement around x, y, and z-axes. We prepared two sets [ventral (θ = 0°) and dorsal view (θ = 180°)] of 10 × 10 tiles of 600 images for each stack with 10% overlap in both x- and y-direction. These images were stitched with TeraStitcher, and the resulting stitched images were downsampled. The downsampled ventral images were registered to the downsampled dorsal images by ANTs. Then Euler angle around x, y, and z-axes, and translation were calculated.

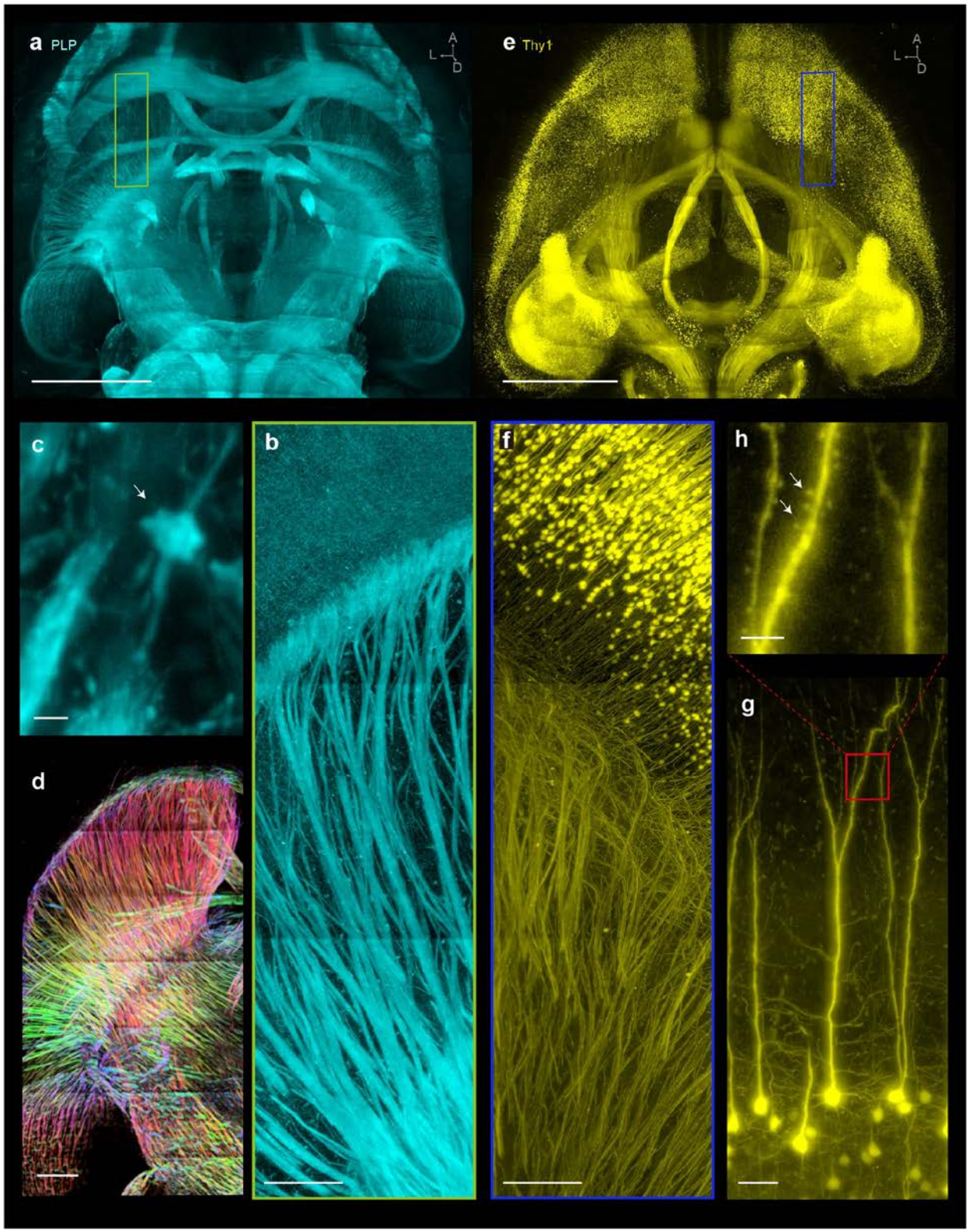
a PLP
A
L
D
e Thy1
A
L
D
c
b
f
h
g
d

Supplementary Figure 10

Whole-brain imaging of a CUBIC-X expanded brain with customized LSFM resolves multiscale cellular structures.

(a) Volume rendered image of PLP-tTA::tetO-ChR2EYFP mouse brain, imaged by customized LSFM. (b) Magnified view of a in the region enclosed in the green box. The maximum intensity projection along V-D axis spanning 500 μm was applied to generate the image. (c) Detailed view of a from the striatum region. Because CUBIC-X highly retains the fluorescent proteins, subcellular structures of a single oligodendrocyte cell (indicated by a white arrow) can be clearly imaged by LSFM. (d) From the images shown in a, the fiber orientations were color-coded by their orientations, which were determined by applying fiber enhancement filter (Online Methods) (e) Volume rendered image of Thy1-YFP-H mouse brain, imaged by customized LSFM. (f) Magnified view of e in the region enclosed in the blue box. The maximum intensity projection along V-D axis spanning 1000 μm was applied to generate the image. (g) Detailed view of e from the cerebral cortex. (h) A magnified view of g in the region enclosed in the red box. Branching of axons as well as single spines (indicated by white arrows) can be clearly resolved by expanding the sample and using the high-resolution LSFM. In b, c, f, g and h, the image intensity was adjusted by taking the logarithms of raw intensity for better visual contrast. For b and f, three image tiles were stitched together by blending the overlapping regions with linear weight using “Pairwise Stitching” plugin in ImageJ. Scale bars indicate 5 mm (a), 500 μm (b), 20 μm (c), 1 mm (d), 5 mm (e), 500 μm (f), 100 μm (g), and 20 μm (h) in the scale of “after-CUBIC-X” brain.

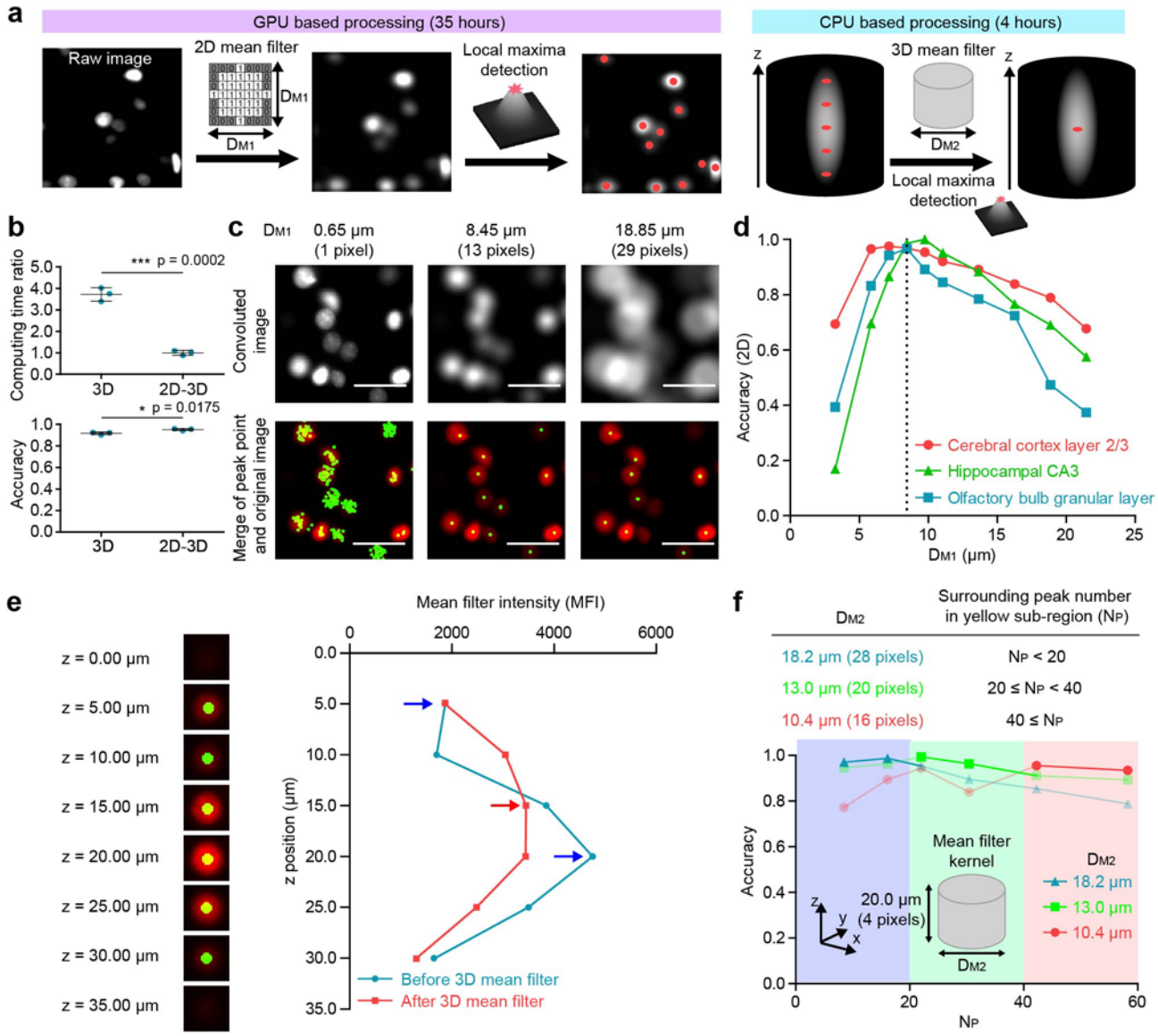

Supplementary Figure 11

A two-step convolution algorithm for the detection of cell nuclei in a whole brain.

(a) Schematic of cell detection of nuclear-stained CUBIC-X brain images. To establish two-step cell-detection algorithm, we first detected individual cells in a 2D xy-plane, and then unified the multiply-detected cells in 3D volume. In each step of this algorithm, we detected local maxima after applying a different mean filter. We used a 2D mean filter kernel with a diameter D_{M1} in the first GPU-based 2D cell-detection step, and 3D mean filter kernel with a diameter D_{M2} in the second CPU-based 3D cell-unifying step, respectively. (b) Comparison of calculation speed and accuracy in cell detection between 3D-based one-step convolution algorithm and our two-step algorithm (***p < 0.001, *p < 0.05, independent two-tailed t-test). The average ± SD were evaluated in the independent three regions. (c) The effect of the first 2D mean filter in cell detection. While no filters [D_{M1} = 0.65 μm (1 pixel)] to the raw data resulted in multiple detections of a single cell, large diameter [D_{M1} = 18.85 μm (29 pixels)] led to the failure in detecting all cells within the image. The accuracy of cell detection depends on mean filter diameter (D_{M1}). Scale bars indicate 50 μm in the scale of an “after-CUBIC-X” brain. (d) The plots of the accuracy of 2D cell-detection against D_{M1} in cerebral cortex layer 2/3, hippocampal CA3, and olfactory bulb granular layer, respectively. We found D_{M1} of 8.45 μm was the optimal value over the three regions. (e) The effect of the second 3D mean filter in cell detection. After 2D cell detection, a single cell was multiply detected over the several stacked images (left). Then, we attempted to unify the multiply-detected points by detecting local maxima of these points in the z-direction. We succeeded in the convergence of the multiply detected points (red arrow; local maxima of after 3D mean filter) after 3D mean filtering while failing to unify these points before 3D mean filtering blue arrow; local maxima of before 3D mean filter. (f) The plots of the accuracy of 3D cell-unification against

surrounding peak number (NP, Online Methods) in the three different D_{M2} value. We note that optimal values for D_{M2} were highly dependent on the density of cells. 13.0 μm for D_{M2} was the most accurate parameter value for the brain region with an intermediated cell density whereas 18.2 μm and 10.4 μm for D_{M2} were the more accurate for those with lower and higher cell density, respectively.

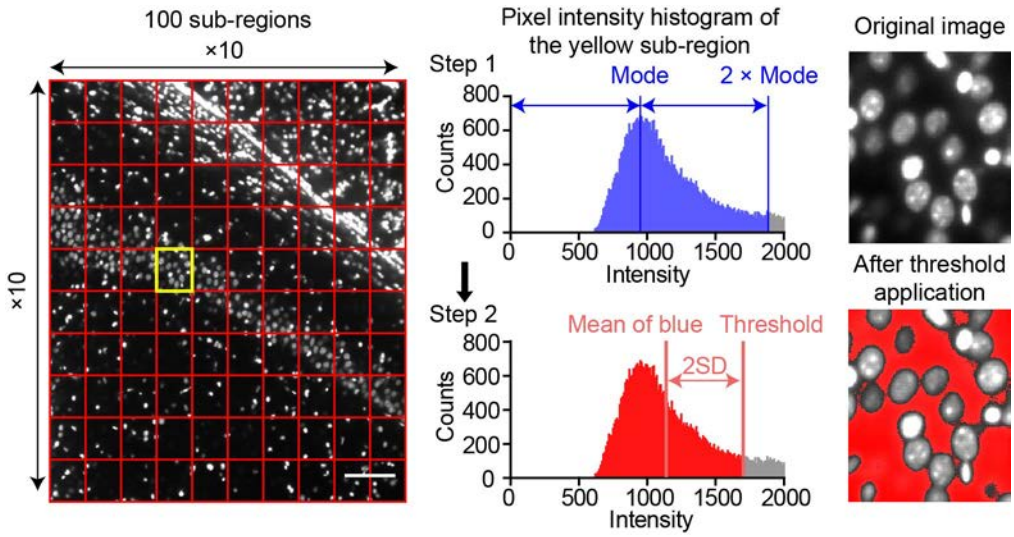

Supplementary Figure 12

The automated determination of an image threshold.

Background threshold was determined by the histogram of pixel intensity in each sub-region (1/100 of the original image) in the 2D cell-detection step. We determined the intensity less than 2 × mode as background intensity, and then extracted background signals (blue). Next, we calculated mean intensity and SD from the resulting histogram, and then determined the intensity less than 2 SD above the mean intensity as an image threshold (red). Scale bars indicate 200 μm in the scale of an “after-CUBIC-X” brain.

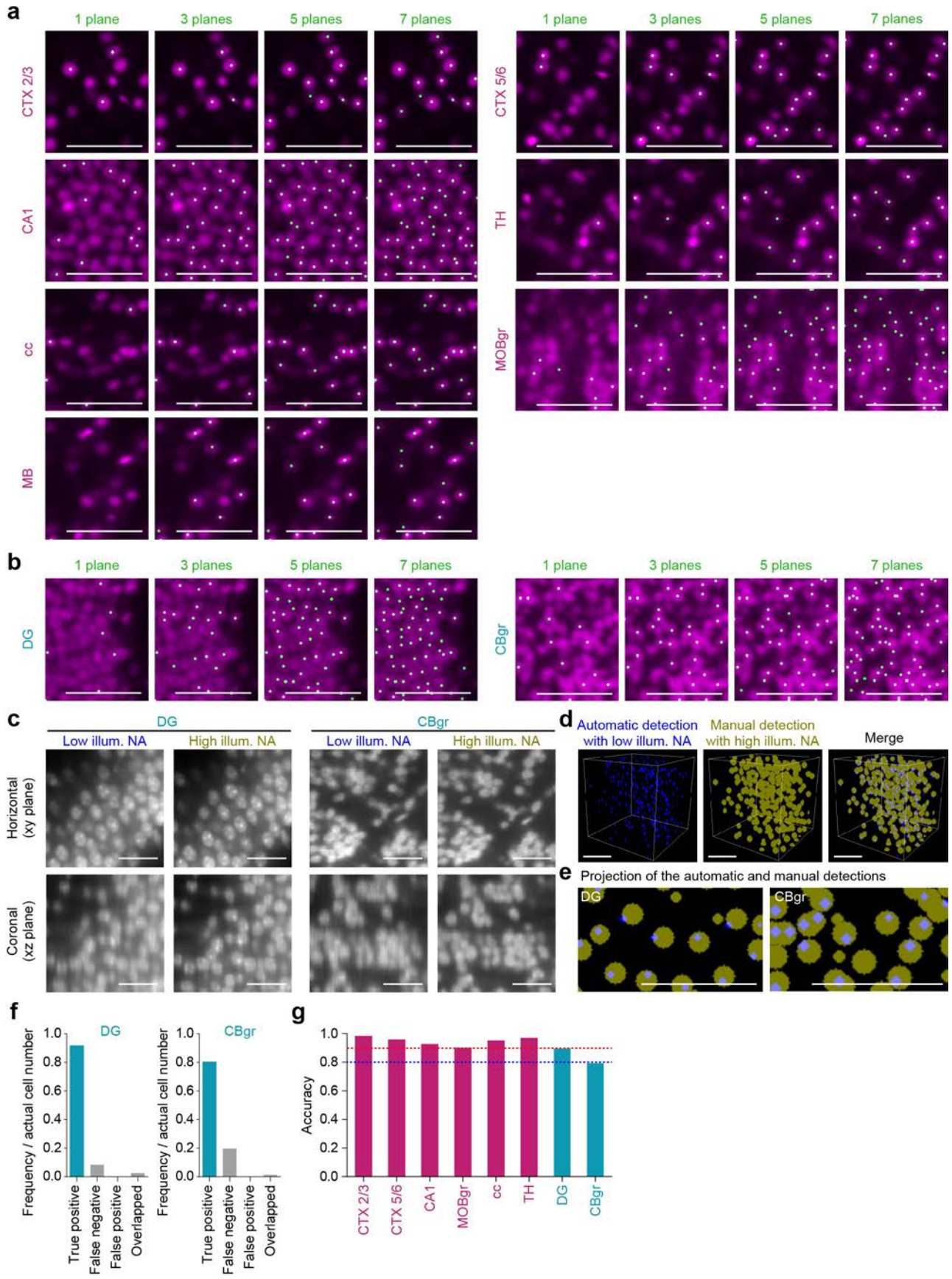
a
1 plane
3 planes
5 planes
7 planes
CTX 2/3
CA1
cc
MB
CTX 5/6
TH
MOBgr
b
DG
CBgr
c
DG
CBgr
Low illum. NA
High illum. NA
Horizontal (xy plane)
Coronal (xz plane)
d
Automatic detection with low illum. NA
Manual detection with high illum. NA
Merge
e
Projection of the automatic and manual detections
DG
CBgr
f
Frequency / actual cell number
True positive
False negative
False positive
Overlapped
g
Accuracy
CTX 2/3
CTX 5/6
CA1
MOBgr
cc
TH
DG
CBgr

Supplementary Figure 13

The evaluation of accuracy for the automated detection of cell nuclei in a whole brain.

(a) The representative images of cell detection in sparsely populated areas. Because cell detection was performed in a three-dimensional manner, the cellular nuclei shown in single planes (magenta) were repeatedly detected in different axial positions. The lateral positions of detected cellular nuclei (green) in surrounding z-planes (1, 3, 5, or 7) were shown in each image. CTX, cerebral cortex; TH, thalamus; cc, corpus callosum; MOBgr, main olfactory bulb granular layer; MB, midbrain. Scale bars indicate 100 μm in the scale of an “after-CUBIC-X” brain. (b) The representative images of cell detection in densely populated areas. DG, dentate gyrus; CBgr, cerebellum granular layer. For a and b, experiments were repeated more than ten times with independent brains. The representative images are shown. (c) Image comparison of low-illumination-NA condition (measured FWHM = 11.0 μm, scanning step size= 5.0 μm) and high-illumination-NA condition (measured FWHM = 5.2 μm, scanning step size= 2.0 μm). Horizontal and coronal sectional images of DG and CBgr are shown. Scale bars indicate 50 μm in the scale of “after-CUBIC-X” brain. Experiments were repeated three times with different brain areas. The representative images are shown. (d) Comparison of the manually annotated nuclei with the automatically detected nuclei. Two people independently annotated the nuclei for manual annotation. Scale bars indicate 50 μm in the scale of “after-CUBIC-X” brain. (e) Projected image of manually annotated nuclei and automatically detected nuclei in DG and CBgr. The projection of 25 μm are shown. Scale bars indicate 50 μm in the scale of “after-CUBIC-X” brain. (f) Details of the accuracy of the automated two-step cell-detection algorithm in DG and CBgr. (g) The accuracy of the cell detection in various brain areas. Red and blue lines indicate 0.9 and 0.8, respectively. For f and g, one and three volumetric images were used for each to evaluate accuracy.

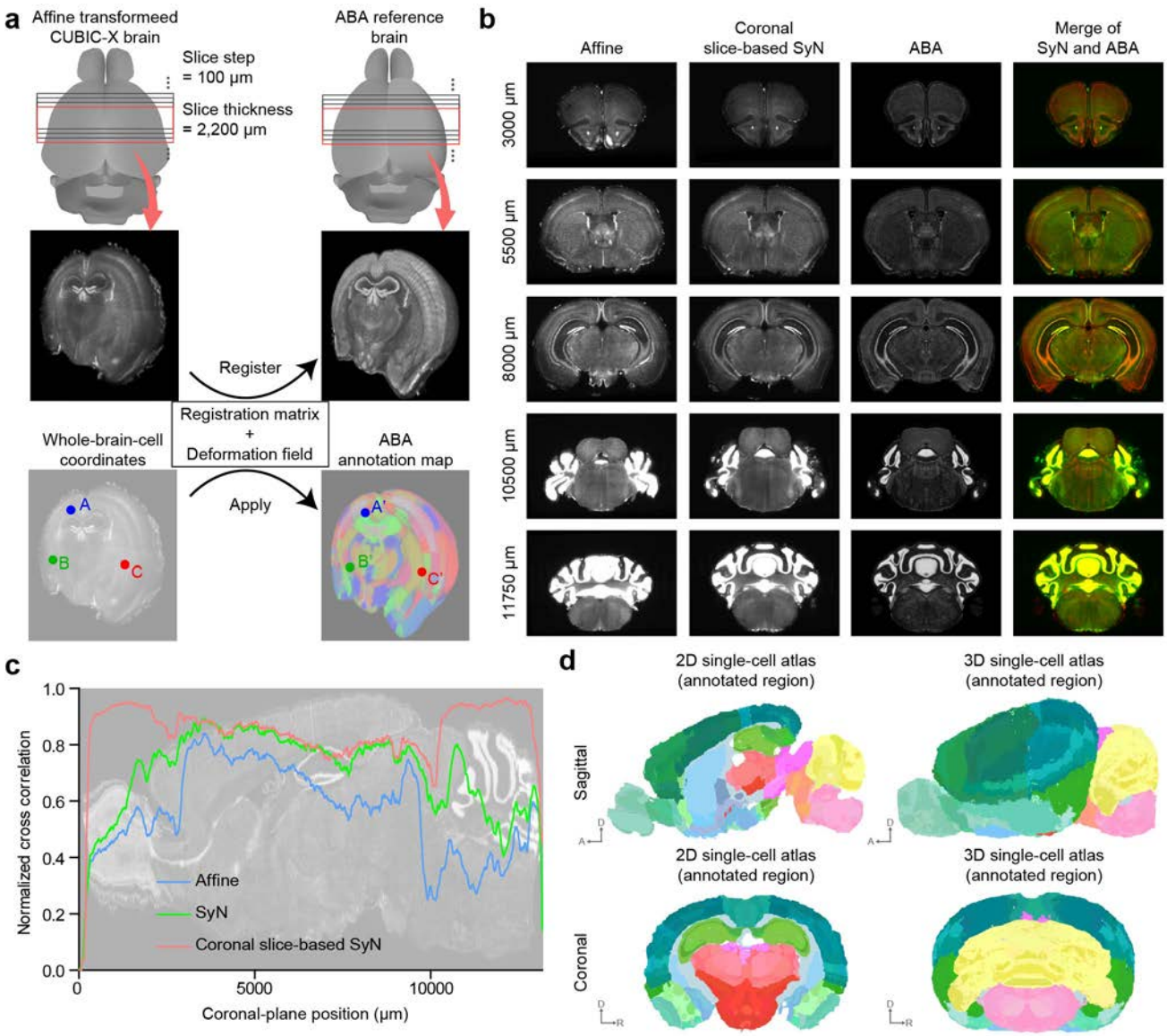

Supplementary Figure 14

Non-linear registration of coronal slices in a CUBIC-X brain to Allen Brain Atlas.

(a) A schematic diagram for the registration of a CUBIC-X brain to an Allen Brian Atlas (ABA) brain based on the virtual coronal slices. After registration of the CUBIC-X brain images by affine transformation, we generated about a hundred overlapping 3D coronal slices with a 2.2-mm thickness at a 100-μm step both from the CUBIC-X and ABA brains. We then registered each coronal-slice image of the CUBIC-X brain onto the coronal-slice images of the ABA brain by non-linear transformation. (b) Coronal single-plane images of a CUBIC-X brain with affine transformation ("Affine"), a CUBIC-X brain with non-linear transformation based on coronal slices ("Coronal slice-based SyN"), an ABA brain ("ABA"), and merged coronal single-plane images of non-linearly transformed CUBIC-X (green) and ABA brains (red). (c) Normalized cross-correlations of a CUBIC-X brain against an ABA brain over entire coronal single-plane positions by straightforward affine transformation ("Affine", blue), straightforward non-linear transformation ("SyN", green), and non-linear transformation based on coronal slices ("Coronal slice-based SyN", red). (d) Sagittal and coronal images of a 2D and 3D single-cell-resolution mouse brain atlas (CUBIC-Atlas) based on an 8-week-old C57BL/6J mouse brain. For non-linear transformation, symmetric normalization (SyN) in ANTs software was used (Online Methods).

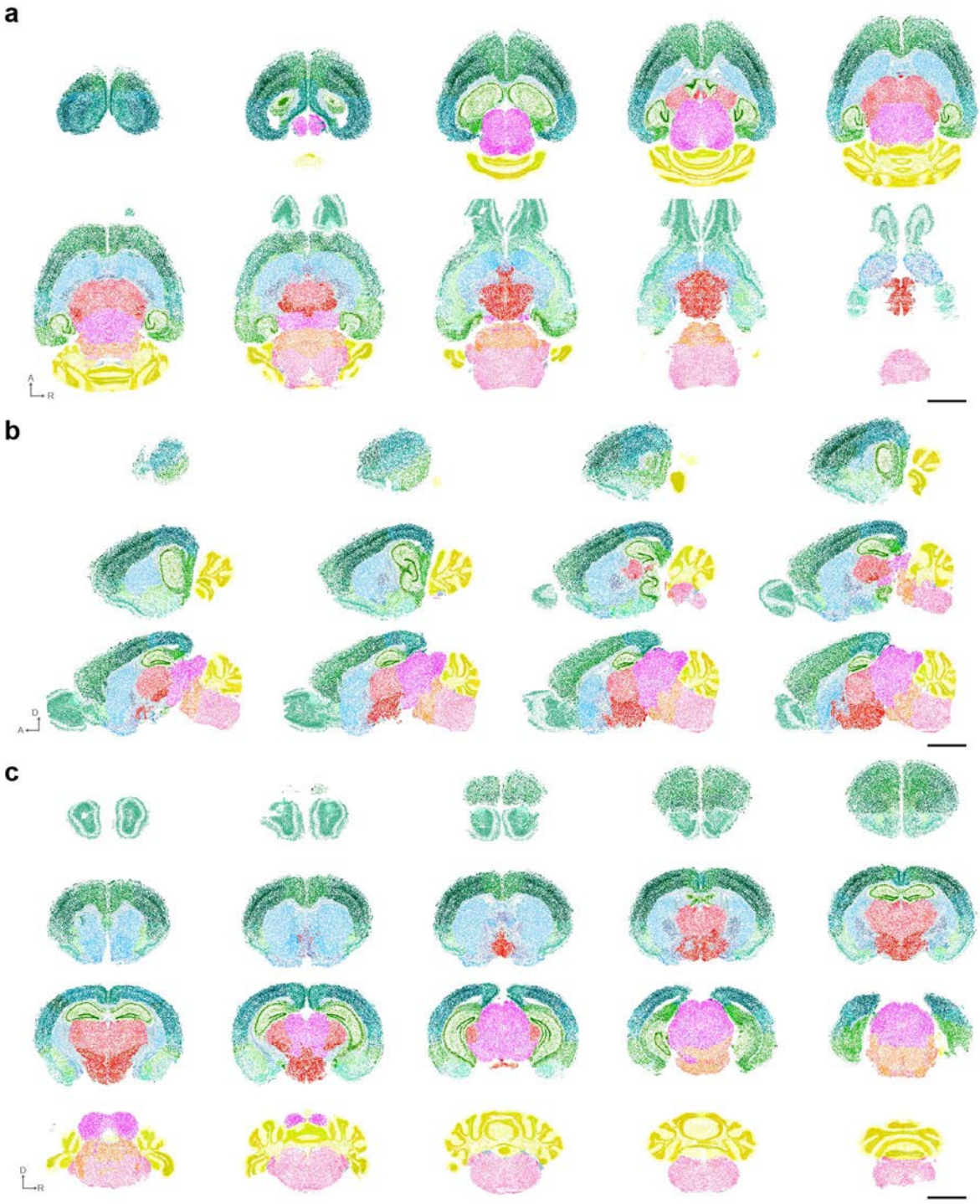

Supplementary Figure 15

A single-cell-resolution mouse brain atlas (CUBIC-Atlas).

(a-c) Horizontal (a), sagittal (b) and coronal (c) single-plane images of CUBIC-Atlas. Each color indicates a corresponding anatomical area (see also Supplementary Table 3 for color). Scale bars indicate 5 mm in the scale of “after-CUBIC-X” brain. Each slice is shown at 1.495 mm (a), 0.845 mm (b) and 0.585 mm (c) step.

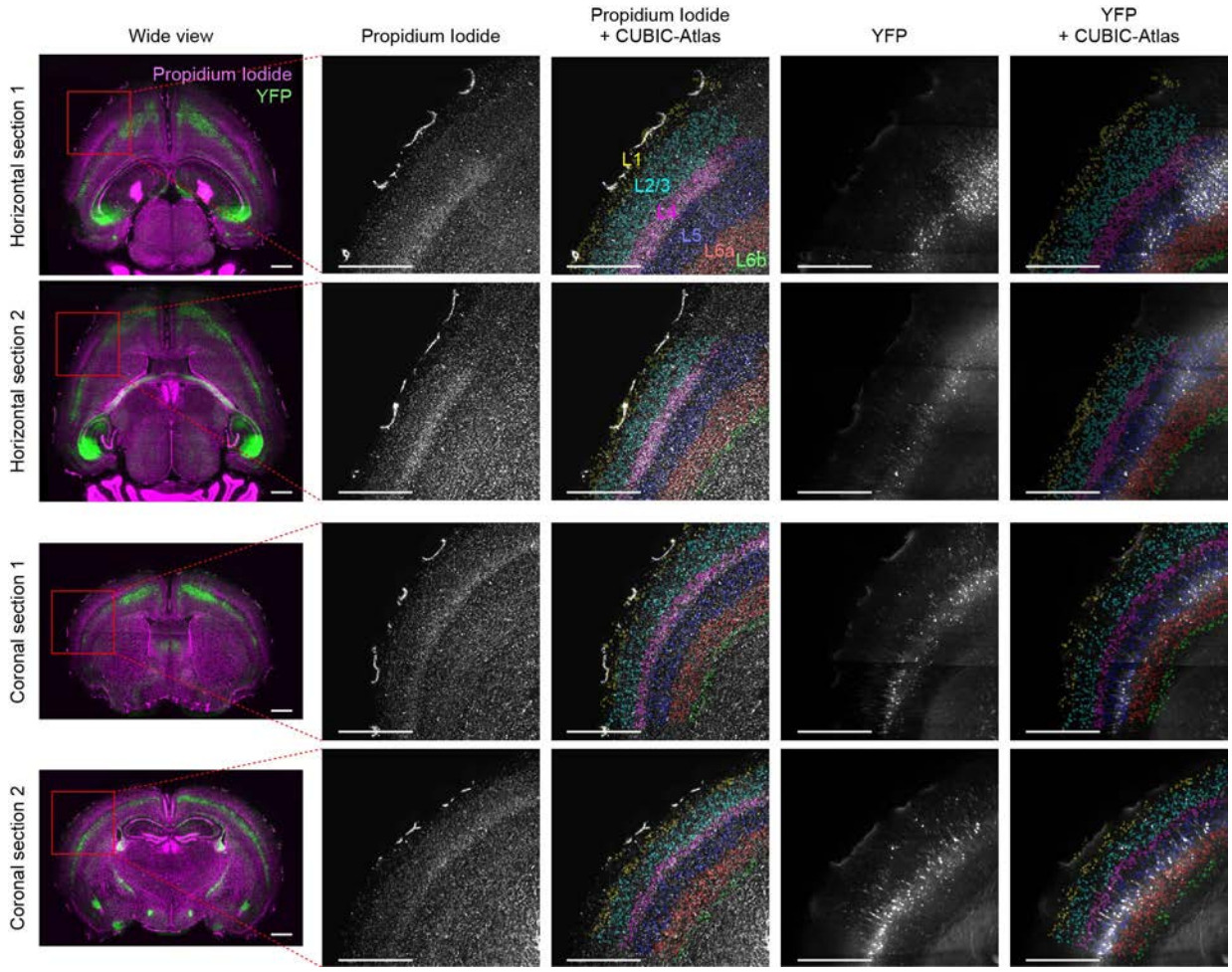

Supplementary Figure 16

Layers of Cerebral cortex in a CUBIC-Atlas overlaid with a PI-stained Thy1-YFP-H mouse brain.

A PI stained Thy1-YFP-H mouse brain was expanded by CUBIC-X and imaged with the customized LSFM. The acquired volumetric images were downsampled, then non-linearly registered to a CUBIC-Atlas. The layer structures of CUBIC-Atlas were overlaid with the images of PI and YFP, respectively. Cerebral cortical layers of somatosensory areas, posterior parietal association areas, and visual areas of a CUBIC-Atlas were visualized with pseudo-color codes. L1, layer 1; L2/3, layer 2/3; L4, layer 4; L5, layer 5; L6a, layer 6a; L6b, layer 6b. Experiments were repeated twice with independent brains and the representative images are shown. Scale bars indicate 2000 μm in the scale of an “after-CUBIC-X” brain.

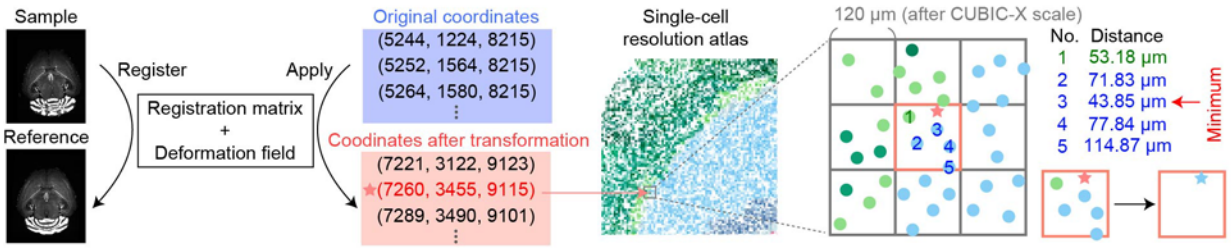

Supplementary Figure 17

Anatomical annotation with CUBIC-Atlas.

After registration, we detected the nearest neighbor cell as a reference in CUBIC-Atlas to the cell of interest in the obtained images. To reduce computational cost, we performed this search in the locally allocated grids (120 μm × 120 μm × 120 μm) partitioned from the atlas space. We annotated the corresponding region of the nearest neighbor cell in CUBIC-Atlas to a region of the cell of interest (Online Methods).

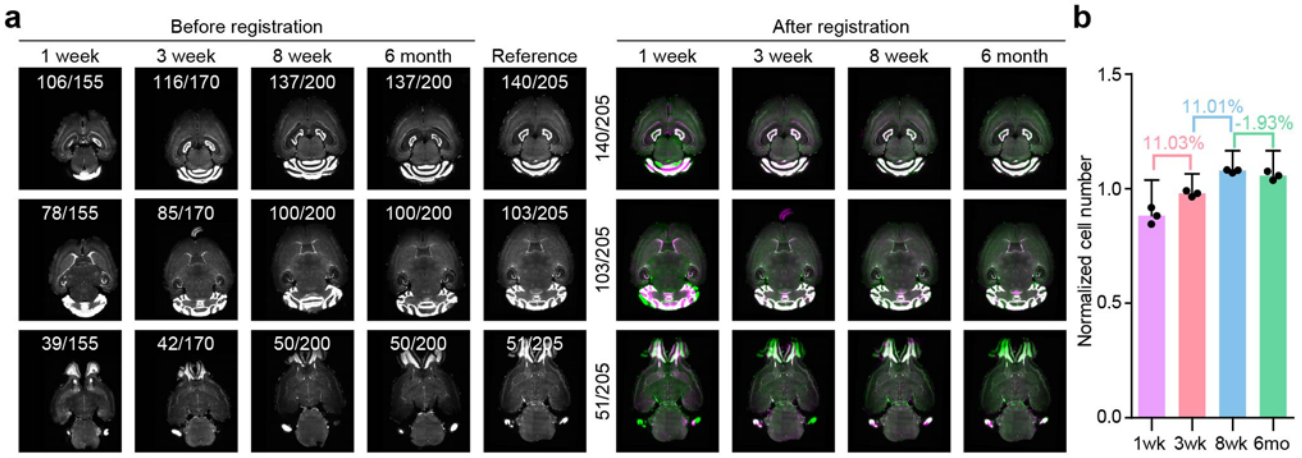

Supplementary Figure 18

Whole-brain cell profiling over different developmental stages.

(a) Horizontal images of CUBIC-X brains of different aged mice before and after registration to CUBIC-Atlas. “Before-registration” images are shown on the left. Indicated numbers mean the horizontal slice positions. In the “After-registration” images, green shows the reference brain and magenta shows the registered brains. (b) Normalized cell number over different aged mice (n = 3). The average ± SD are shown.

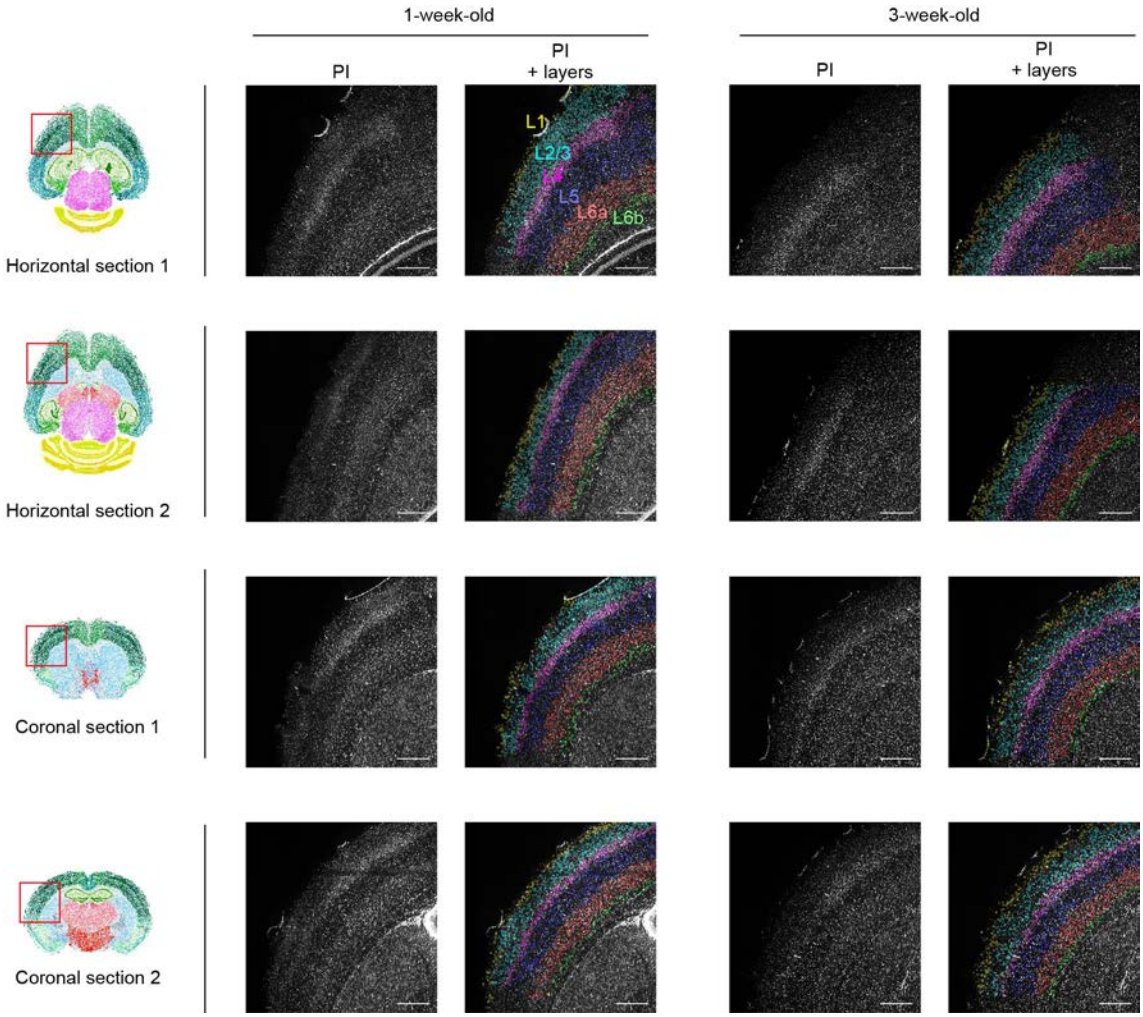

Supplementary Figure 19

Mapping of 1-week-old and 3-week-old mice brains onto a CUBIC-Atlas.

PI-stained 1-week-old and 3-week-old mice brains were mapped onto and annotated with a CUBIC-Atlas based on an 8-week-old mouse brain. Cerebral cortical layers of somatosensory areas, posterior parietal association areas, and visual areas with annotations are visualized with pseudo colors. On the left, red squares indicate the approximate positions of the magnified brain regions shown in the right. Experiments were repeated three times with independent brains. The representative images are shown. L1, layer 1; L2/3, layer 2/3; L4, layer 4; L5, layer 5; L6a, layer 6a; L6b, layer 6b. Scale bars indicate 1000 μm in the scale of an “after-CUBIC-X” brain.

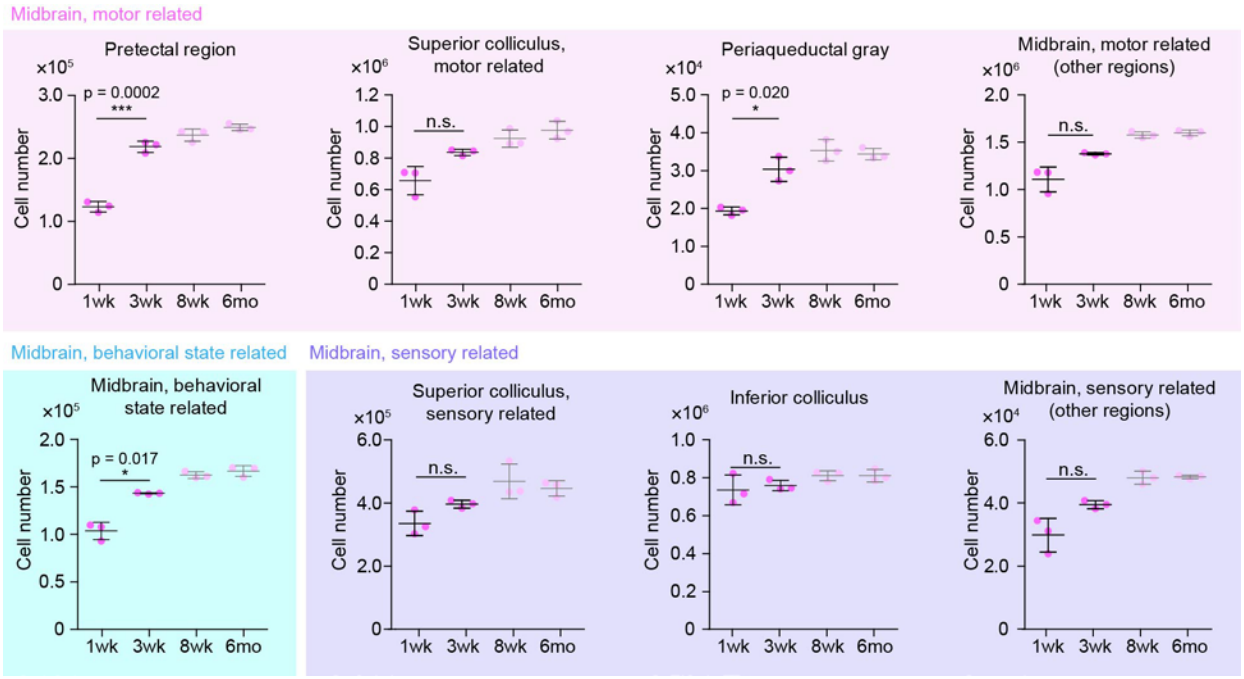

Supplementary Figure 20

Whole-brain cell profiling over different developmental stages in midbrain.

The significant increase of the total cell number in the midbrain (n = 3, ***p < 0.001, *p < 0.05, independent two-tailed t-test). Background color represents each classification of the midbrain (Pink for motor-related areas, blue for behavioral-state-related areas and purple for sensory-related areas, respectively). The average ± SD are shown.

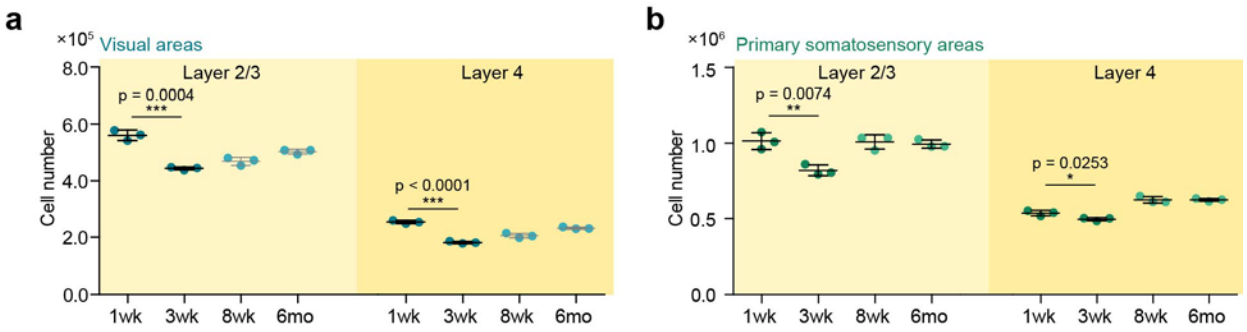

Supplementary Figure 21

Whole-brain cell profiling over different developmental stages in cerebral cortex.

The significant decrease in the total cell number in visual areas (a) and primary somatosensory areas (b) of the cerebral cortex areas (n = 3, *** $p < 0.001$, ** $p < 0.01$, * $p < 0.05$, independent two-tailed t-test). The average ± SD are shown.

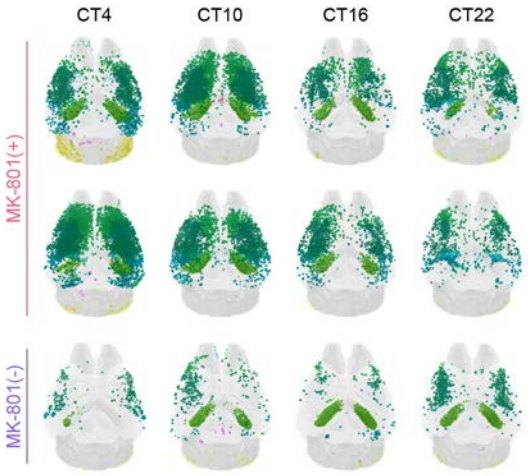

Supplementary Figure 22

Probabilistic mapping of pharmacologically stimulated mouse brains expressing an Arc-dVenus reporter onto a CUBIC-Atlas.

Temporal variation of distribution of hyper-activated cells in the whole brain. Original image data were obtained in Tatsuki et al. (Online Methods), and re-analyzed in this study. Arc-dVenus expressing cells in mice with or without the chronic administration of MK-801 are shown. The color represents an anatomical area of the detected cells. All brain samples used in the experiment are shown except the brain samples shown in Fig. 7b.